Thermo-mechanical modelling of stress relief heat treatments after laser-based powder bed fusion

De Baere, David; Van Cauwenbergh, Pierre; Bayat, Mohamad; Mohanty, Sankhya; Thorborg, Jesper; Thijs, Lore; Van Hooreweder, Brecht; Vanmeensel, Kim; Hattel, Jesper H.

Published in:
Additive Manufacturing

Link to article, DOI:
10.1016/j.addma.2020.101818

Publication date:
2021

Document Version
Publisher's PDF, also known as Version of record

Additive Manufacturing 38 (2021) 101818

Contents lists available at ScienceDirect

Additive Manufacturing

journal homepage: www.elsevier.com/locate/addma

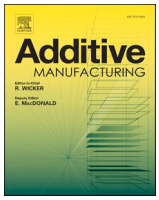

Research Paper

Thermo-mechanical modelling of stress relief heat treatments after laser-based powder bed fusion

David De Baere [a,*], Pierre Van Cauwenbergh [b], Mohamad Bayat [a], Sankhya Mohanty [a], Jesper Thorborg [a], Lore Thijs [b], Brecht Van Hooreweder [c], Kim Vanmeensel [d], Jesper H. Hattel [a]

[a] Department of Mechanical Engineering, Technical University of Denmark, Produktionstorvet, Building 425, 2800 Kgs. Lyngby, Denmark
[b] 3D Systems Leuven, Grauwmeer 14, 3001 Leuven, Belgium
[c] KU Leuven, Mechanical Engineering Department, Celestijnenlaan 300 box 2420, 3001 Leuven, Belgium
[d] KU Leuven, Materials Engineering Department, Kasteelpark Arenberg 44 box 2450, 3001 Leuven, Belgium

A B S T R A C T

Laser-based powder bed fusion, due to its layer-by-layer nature, results in a unique stress profile in a part after the primary production process. The residual stresses are typically tensile near the top, while they are compressive near the bottom of the part. When it is removed without proper precautions, the part will bend excessively. In order to alleviate this deformation, a stress relief heat treatment can be applied. In this paper, such a stress relaxation heat treatment is modelled to investigate the effect of the post-processing parameters. The model uses an Arrhenius-type creep equation to simulate the influence of the heat treatment temperature and dwell time on the stress field in a relatively simple cantilever beam produced in Ti-6Al-4V. Via validation of the simulations, the effect of the heat treatment is shown to be represented accurately. The validated model is used to predict the deformation that results from the residual stresses after heat treating the part under various conditions. The results from the simulations ultimately allow choosing the optimal heat treatment conditions to obtain a given reduction in the residual stress level, while reducing the need for extensive experimental investigations.

1. Introduction

Additive manufacturing of metals allows the production of parts with a high complexity or low production volume at a limited cost. In laser-based powder bed fusion (LPBF), which is a type of metal additive manufacturing, the part is built up from metal powder. The LPBF machine spreads a thin layer of material on a build plate, and a laser melts the cross-section of the desired part in the powder layer. Subsequently, the build plate is lowered by one step, and a new layer of powder is distributed. This process repeats until the part is completed [1].

Due to this layer-by-layer method of producing the part, the stress changes throughout. One particular part of the residual stress is caused by thermal contraction. When a layer is just deposited, its temperature is higher than underlying ones, and hence, it is expanded. Because it is attached to the underlying layers, the top-most layer is compressed, and it exerts a tensile stress on the region underneath it. However, when cooling down, the new layer cools down and contracts more than earlier deposited layers, causing tensile residual stresses in this final layer, and compressive ones near the bottom of the part [2]. When cutting the part from the base plate, part of the residual stresses are released, which can lead to deformation [3–5]. Other mechanisms will also affect the residual stress state, and therefore the final deformation. For example, differential contraction in neighbouring scan tracks also cause residual stresses, but these typically do not affect the deformation as much as the layer-based ones [6,7].

To address this issue of deformation, a part produced by additive manufacturing is typically heat treated before it is removed from the build plate. Stress relaxation typically occurs due to one of two mechanisms [8]. Heating up the part reduces the yield strength. This reduction in the yield stress will cause the stress to relax due to plastic yielding. A second mechanism taking place is creep, which is only activated at higher temperatures, and represents a time-dependent stress reduction [8]. The reduction of the residual stress also increases the toughness of the part by removing high tensile stresses at the surface [9].

However, heat treatment is an expensive process, since it requires the part to be heated up in a furnace to the heat treatment temperature, and kept at this temperature for an extended period of time. Therefore, there is a need to find the optimal parameter set, both in terms of dwell time, and heat treatment temperature [10]. Additionally, the unique microstructure and residual stress state resulting from the LPBF process allow the part to have novel properties, but require the development of novel heat treatment processes. Two approaches can be followed to find this

* Corresponding author.
E-mail address: ddbae@mek.dtu.dk (D. De Baere).

https://doi.org/10.1016/j.addma.2020.101818
Received 26 August 2020; Received in revised form 23 October 2020; Accepted 21 December 2020
Available online 8 January 2021

optimal parameter set. Typically, users perform trial-and-error experiments. These experimental studies are slow and costly, since they require several parts being built and post-processed, and cannot guarantee that the found set of parameters is the optimal one. An alternative route is a numerical model. A well-calibrated numerical model can be evaluated multiple times, and using either statistical techniques, such as Monte-Carlo sampling [11], or a generic parametric study, an optimal set of heat treatment parameters can be defined. Of course, calibration still requires some experiments to be performed, which shows that a combined numerical-experimental approach is a time and cost effective approach for finding parameter sets for these new process chains.

The mechanical and thermal properties of the material used for LPBF are of major importance to the followed post-processing, due to their influence on the residual stresses [12], and on the possible changes in microstructure which could follow when transformation temperatures are superseded [13]. In the current study, a part produced by LPBF in Ti-6Al-4V is investigated. Ti-6Al-4V has good mechanical properties, owing to its two-phase equilibrium microstructure. Additionally, titanium alloys have a low density and good corrosion resistance due to the formation of oxides at their surface [14].

Kruth et al. [15] showed that a stress-relief heat treatment at just below 600 °C reduces the deformation due to residual stresses by 80%. Wang et al. [16] investigated stress relaxation occurring during a heat treatment at 600 °C and 700 °C using neutron diffraction. They found that the majority of the stress is relieved within the first ten minutes. Additionally, they identified that the stress is reduced to a few percent after two hours of stress relaxation, indicating complete relaxation of the residual stresses. Additionally, several investigations into the effect of pre-heating the build plate or the build chamber have been executed [17–19]. Denlinger et al. [20] and Ganeriwala et al. [21] investigated the stress relaxation that occurs during the LPBF process itself, using a stress cut-off and visco-plasticity respectively. De Baere et al. [22] investigated the effect of the phase transformation resulting from an intrinsic heat treatment on the residual stress. However, a comprehensive study into the influence of common heat treatment parameters, such as dwell time or heat treatment temperature, and a quantification of the results in, for example, a response surface model remain missing in literature. An earlier investigating into a process chain model for the LPBF process chain by De Baere et al. [23] attempted to remedy this hiatus, but the model was insensitive to the dwell time and temperature due to a lack of a rigorous representation of the time and temperature dependent stress relaxation. Finally, Williams et al. [24] modelled and measured the effect of a stress relaxation heat treatment at 700 °C for 316 L stainless steel, and found a good agreement between the simulations and the neutron diffraction measurements, even though their material properties were measured at a lower temperature.

Looking at alternative processes, modelling of stress relaxation heat treatment is commonly performed for welding. Yan et al. [25] used an Arrhenius-type creep model. They showed a good agreement between the measured and simulated residual stress after the stress relaxation heat treatment. Additionally, they showed that, for the simulated post process, creep is the major contribution factor to the relaxation of residual stress. Dong and Song [26] also found that creep is the dominant mechanism during stress relaxation, and identified that the extent to which the reduction in yield stress contributes to the stress relaxation depends on the ratio between the yield stress and Young's modulus, both at room and the heat treatment temperature. Dong and Hong [27] investigated the effect of the holding time and the effect of the thermal lag that occurs during the ramp-up to the heat treatment temperature. They found that significant stress relaxation occurs during the ramp-up period of the heat treatment, and that creep is the predominant mechanism. Alberg and Berglund [28] compared five different material models to simulate a stress relaxation heat treatment. They found that the choice of creep model does not have a profound effect on the deformation of the part. Moreover, they advise the use of the Norton model, since data is freely available in literature, and only a limited amount of material testing needs to be performed. Finally, the comprehensive review article by Rae [29] concludes that the area of numerical modelling of stress relaxation in Ti-6Al-4V requires more research.

As suggested by these earlier studies, this work will employ a creep-based equation for simulating the time- and temperature effects occurring during a post-LPBF stress relief heat treatment. This study will analyse this model to find the effect of dwell time and heat treatment on the residual stresses in a cantilever produced by LPBF and show which parameter sets lead to a fully relaxed part. The simulations performed for this work represent the new state-of-the-art in terms of modelling stress relaxation heat treatment after the LPBF process, coupling both the flash heating method and a Norton's power law based creep model for the heat treatment. This investigation into the underexplored field of numerical modelling of post-LPBF heat treatment provides the tools to gain insight into the effect of heat treatment temperature and dwell time on the residual stresses in a part produced using an LPBF process chain.

2. Numerical model

In this work, the stress relaxation heat treatment of a part produced by LPBF is simulated in the commercial software suite Abaqus CAE. The part under investigation is a simple supported cantilever beam, since this part has the advantage of a relatively simple deformation profile. Moreover, a cantilever beam, as presented in Fig. 1, will bend in the x-z-plane after release from the build plate. This specific deformation is caused by the tensile residual stress at the top of the beam and the compressive stress at the bottom [30]. The vertical supports are required to make the part printable.

To model a stress relief heat treatment, a two-part model is required. The model needs to capture the change in temperature that occurs during the heat treatment (involving heating up from room temperature, dwell time at the desired temperature, and cooling down to room temperature), and the effects this has on the stresses and strains in the part. To achieve this, the model, implemented in this study, consists of a thermal part, and a mechanical part. Often, studies simulating the LPBF process are based on the inherent strain method [31]. To avoid the machine dependency that arises from the usage of the inherent strain method, the present study uses the first-principle based flash heating method to simulate the primary LPBF process. Both the simulation for the primary LPBF process and the post-LPBF stress relaxation heat treatment use the equations outlined in this section.

2.1. Thermal model

To obtain the temperature field during the heat treatment, the transient heat conduction equation is solved during each increment:

$$\rho C_p \frac{\partial T}{\partial t} = \frac{\partial}{\partial x}\left(k\frac{\partial T}{\partial x}\right) + \frac{\partial}{\partial y}\left(k\frac{\partial T}{\partial y}\right) + \frac{\partial}{\partial z}\left(k\frac{\partial T}{\partial z}\right) \quad (1)$$

where T is the temperature, ρ the density, C_p the specific heat capacity and k the thermal conductivity.

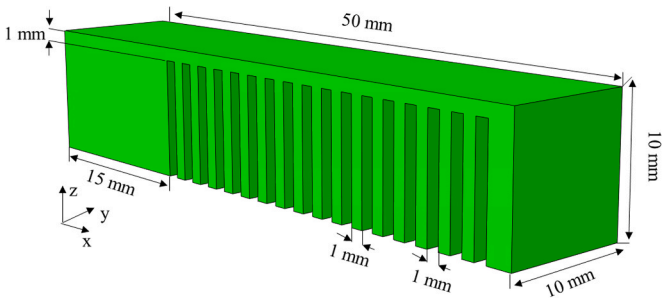

Fig. 1. Simulated part with the relevant dimensions.

2.2. Mechanical model

The mechanical model solves static equilibrium for the stress σ

$$\sigma_{ij,i} = 0 \tag{2}$$

together with the generalised Hooke's law:

$$\sigma_{ij} = \frac{E}{1+\nu}\left[\frac{1}{2}\left(\delta_{ik}\delta_{jl} + \delta_{il}\delta_{jk}\right) + \frac{\nu}{1-2\nu}\delta_{ij}\delta_{kl}\right]\epsilon^{el}_{kl} \tag{3}$$

where E is the Young's modulus, ν the Poisson ratio, δ_{ij} the Kronecker delta and ϵ^{el}_{kl} the elastic strain. The Young's modulus and Poisson ratio are temperature dependent, and therefore change depending on the temperature calculated from Eq. (1). i, j, k and l are the indices for the tensor notation.

The total strain is the sum of all the different strain components. In particular, the total strain is represented in Eq. (4):

$$\epsilon^{tot} = \epsilon^{el} + \epsilon^{pl} + \epsilon^{th} + \epsilon^{cr} \tag{4}$$

with ϵ^{pl} being the plastic strain, ϵ^{th} the thermal strain, and ϵ^{cr} the creep strain. The thermal strain is calculated from a temperature dependent, isotropic thermal expansion coefficient:

$$\dot{\epsilon}^{th} = \alpha\Delta T \tag{5}$$

where α is the thermal expansion coefficient. The contribution of the plastic strain is calculated using J2 flow theory:

$$\Delta\epsilon^{pl}_{ij} = \frac{9}{4\sigma_e^2}\left[\frac{E-E_t}{EE_t}\right]s_{ij}s_{kl}\Delta\sigma_{kl}. \tag{6}$$

The plastic strain increment depends on the effective stress, σ_e, tangent modulus E_t, deviatoric stress components, s_{ij} and Young's modulus, E.

In this work, the stress relaxation is mimicked by using a well-established creep equation. Creep is generally defined as time dependent plastic deformation under a constant mechanical load [32]. According to this definition, stress relaxation is not a pure creep process, since the stress varies as function of time. Moreover, the goal of the stress relaxation heat treatment is to reduce the stresses, while fixing the displacement of the part. Nevertheless, an Arrhenius-type creep law has successfully been used [25] for describing a stress relaxation heat treatment, since such a heat treatment takes place over a long time, typically several hours. As a result, applying this creep equation during each simulation time step is a reasonable assumption. An additional advantage of using a creep equation is that the framework in commercial finite elements software is well developed, and implementation of such an equation is relatively straightforward.

The creep equation in this work is based on Norton's power law [33]:

$$\dot{\epsilon}^{cr} = m\sigma^n \tag{7}$$

where $\dot{\epsilon}^{cr}$ is the creep strain rate and m and n the material constants of the metal under investigation. Yan et al. [25] show that, in order to accurately model the change in the residual stresses after welding, the temperature needs to be taken into account explicitly. This can be accomplished by expanding the prefactor in Eq. (7):

$$m = C\exp\left(-\frac{Q}{RT}\right) \tag{8}$$

where C is the temperature independent prefactor, Q the activation energy for stress relaxation, R the universal gas constant and T the temperature, calculated in Eq. (1). Combining Eqs. (7) and (8) leads to [25]:

$$\dot{\epsilon}^{cr} = C\exp\left(-\frac{Q}{RT}\right)\sigma^n \tag{9}$$

Additional mechanisms, such as cracking, damage and defect formation are not included in the simulations. Although they are of importance [34] for determining the service life of parts produced by LPBF, this is beyond the scope of the present work, but will be included in future modelling efforts.

2.3. Initial residual stress field

In order to evaluate the effect of the heat treatment, it is important to have a sufficiently accurate residual stress field, since the extent to which the stress will be relaxed depends on the initial stress. In this work, the initial residual stress field is obtained from a process simulation using the model put forward by Bayat et al. [35]. A short synopsis of this model is provided. The LPBF simulation uses the so-called flash heating (FH) method to approximate the laser heat input into the top surface of the part. For FH, a number of real layers, together called a meta-layer, is activated, and in the top-most one, a heat source is activated, which is equivalent to the total energy, to which the real layers are exposed. The meta-layer is subsequently allowed to cool down, and afterwards, the next meta-layer is activated. This process repeats until the entire part is built.

The thermo-mechanical model for the initial residual stress field solves the same equations as the model presented for the heat treatment model (specifically Eqs. (1–5)). A more detailed description and investigation of the model used to obtain the stress field can be found in the work by Bayat et al. [35]. Since this work focusses on the stress relaxation heat treatment following the LPBF process, no detailed description of this model is provided, but the residual stress field after the LPBF will be validated with experimental results, showing that the numerical simulation adequately captures the primary process.

2.4. Modelling methodology and boundary conditions

In this work, both the real and simulated part are cantilever beams. The dimensions for the simulated part are given in Fig. 1. The model is composed of three main parts: importing of the initial stress, stress relaxation heat treatment and release of the part from the base plate. The initial stress follows from the initial FH simulation. The advantage of importing the stress separately rather than integrating the FH simulation in a LPBF process chain model is that it saves computational cost. This paper will investigate the effect of the dwell time and heat treatment temperature. Importing the stress reduces the need for resimulating the primary LPBF process itself.

The effect of the heat treatment is evaluated at five different temperatures and for six different dwell times each. The temperature profile,

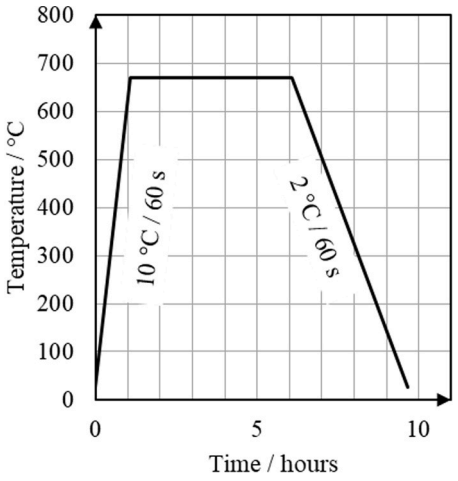

Fig. 2. Temperature profile during the stress relaxation heat treatment model at 670 °C.

shown in Fig. 2, is applied in two boundary conditions to all faces exposed to the furnace. Both radiation and convection are considered, with an emissivity of 0.4 and convective heat transfer coefficient of 10 W m^{-2} K^{-1} [25]. All other boundary conditions are adiabatic.

Finally, the part is cut from the base plate. This reveals the effect of the residual stress on the deformation. The cutting operation is mimicked by using the model change interaction in Abaqus CAE. The supports are removed from the simulation, and the residual stress is released, until the part reaches a new equilibrium through deformation.

3. Experimental measurements

To validate the simulations a number of dedicated experiments is performed. These experiments consist of printing the cantilever geometry, and applying a heat treatment. The parts are subsequently cut from the base plate, and the deformation is measured and used as a metric for evaluating the effect of the heat treatment.

In the present work, a 3D Systems® DMP Flex 350 was used to build the samples. The machine is equipped with a fibre laser with a power of 500 W and a Gaussian energy distribution. The samples were built with a layer thickness of 30 μm, and a volumetric energy density of 67.1 J mm^{-3} was applied. The DMP Flex 350 applied a random incremental scan rotation when printing the samples. The stress relief heat treatment for validation of the simulations was performed at 670 °C in an argon atmosphere. To reach this temperature, a heating rate of 10 °C per minute was prescribed to the furnace. The dwell time for the heat treatment was five hours, followed by furnace cooling. The cooling and heating rates for the experimental heat treatment are the same as the ones used for the simulations. Four cantilevers were built in total, in different configurations. Fig. 3 shows the 3DXpert CAD file used for printing the cantilevers.

The cutting process used wire electrical discharge machining (EDM) to separate the cantilever from the build plate. This operation was performed using a Wire EDM AgieCharmilles CUT AM 500. To evaluate the deformations resulting from the release of the residual stresses caused by cutting the part from the base plate, a 3D-scan of the cantilever was taken with an optical GOM ATOS Core 3D-scanner and analysed with the GOM inspect software. To assess the deflection of the cantilever beam, three vertical cross-sections are extracted from the 3D scan, and a circle is fitted through the top surface of each of these. This assures that roughness and other surface texture effects are not affecting the measured deflections, since this study investigates the deformations caused by the macroscopic residual stresses.

4. Material parameters

The investigated material in this study is Ti-6Al-4V ELI, with a chemical composition compliant with ASTM F3302. The composition is shown in Table 1. This material can be additively manufactured and has good specific mechanical material properties and corrosion resistance [36]. The thermo-mechanical material properties are derived from the works by Bayat et al. [35], Ganeriwala et al. [21] and Yan et al. [25], and are shown in this section.

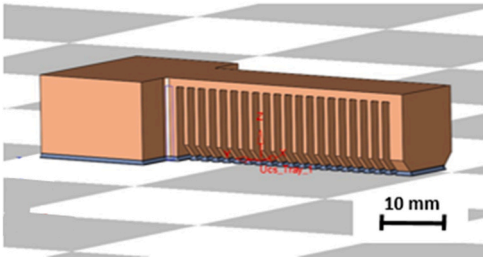

Fig. 3. 3DXpert CAD file used for printing the cantilevers.

4.1. Thermal properties

The thermal properties for the simulations are shown in Table 2. Only the specific heat is dependent on temperature.

4.2. Mechanical properties

The mechanical properties are displayed in Table 3. Additionally, the temperature dependent yield stress and Young's modulus are shown in Fig. 4. All material properties in Table 1 and Table 2 were derived from experiments and their use for numerical modelling of Ti-6Al-4V was validated in their original sources. Since the material properties were derived for the processes they are simulating, they represent an averaged value for all the phase transformations that can take place during the process. For example, in Ti-6Al-4V, the expected martensitic microstructure will decompose into a mix of the equilibrium phases, α and β. This transformation corresponds to a change in mechanical and thermal material properties, which can be the subject of a future study aiming at improving the input for numerical simulations of Ti-6Al-4V.

5. Results and Discussion

5.1. Initial residual stress field

In order to investigate the effect of the stress relaxation heat treatment on the residual stresses, a realistic initial field is required. This stress field follows from the process simulation in Abaqus CAE for the LPBF process itself. The model used for this initial stress field is outlined in Section 2.3. The stress field (more specifically the normal component in the direction of the beam, from now on called σ11) is shown in Fig. 5. Focussing on the cantilever beam itself, σ11 varies from tension near the top of the beam to compression near the bottom. However, since the top surface is a free surface, the tensile stress is higher just below it. The highest tensile stress in the cantilever beam is located at the bottom of the top-most meta-layers, which is approximately 0.5 mm from the top of the beam. Additionally, there are two regions of high tensile stress near the bottom corners of the left-most support. The stripe-like pattern visible in the residual stress field is caused by the meta-layer depositing. Bayat et al. [35] investigated the effect of the chosen settings of the flash heating method, and showed that the chosen mesh and meta-layer thicknesses do not majorly affect the resulting stress field.

The main method of validating the initial stress field will be through the measurable deformation following from the residual stress field. This requires a cutting step, both in the experiments and the numerical model. Fig. 6 shows the total deformation of the cantilever after its support is removed using the model change interaction. Using a cantilever beam assures that the majority of the deformation is located in the beam itself. This is also evident from Fig. 6, which shows a deformation of less than 0.2 mm in the left-most support. However, the tip of the cantilever bends up approximately 2 mm. This deformation is similar to simulated and measured results in other studies for similar cantilever geometries. For example, Setien et al. [31] measured a displacement between 1.8 mm and approximately 4 mm, depending on the scanning strategy. Both Yakout et al. [12] and Chen et al. [37] simulated and measured displacements below 2 mm for a beam of a similar length and from the same material (Ti-6Al-4 V), but with a larger beam thickness. In the next section, experimental validation is provided for the simulated deformation field.

In the following paragraph, the residual stresses in Fig. 5 are compared to measurements in Ti-6Al-4V from literature. Yadroitsava et al. [38] identified the range of the residual stresses at the surface of a part produced by LPBF. A residual stress with a maximum value of approximately 650 MPa and a minimum of 300 MPa was measured in their study for a part with a height similar to the cantilever simulated in this work. This indicates that the results from the flash heating simulation correspond to expectations from experimentally obtained values.

Table 1
Composition of Ti-6Al-4V ELI according to ASTM F3302.

Element	C, max	O, max	N, max	H, max	Fe, max	Al	V	Y, max	Other
Composition in wt%	0.08	0.13	0.05	0.012	0.25	5.50–6.50	3.50–4.50	0.0005	0.40

Table 2
Thermal material properties. Data from [21,35].

Parameter	Value	Units	Symbol	
Thermal Conductivity Below Solidus Temperature	13	W m^{-1} K^{-1}	k	
Thermal Conductivity Above Liquidus Temperature	33	W m^{-1} K^{-1}		
Latent Heat of Melting	186	kJ kg^{-1}	ΔH_f	
Solidus Temperature	1620	°C	T_s	
Liquidus Temperature	1654	°C	T_l	
				Temperature / °C
Specific Heat Capacity	543	J kg^{-1} $°C^{-1}$	C_p	20
	543			1620
	750			1654
	750			3000

Table 3
Mechanical material properties. Data from [21,25,35].

Parameter	Value	Units	Symbol		Source
Density	4400	kg m^{-3}	ρ		[21, 35]
Poisson's Ratio	0.33	/	ν		[21, 35]
Plastic Tangent Modulus	8.0	GPa	E_t		[21, 35]
Creep Exponent	3.6766	/	n		[25]
Creep Coefficient	9.87e-10	s^{-1} $Pa^{-3.6766}$	A		[25]
Creep Activation Energy	419.9	kJ mol^{-1}	Q		[25]
Universal Gas Constant	8.3145	J $°C^{-1}$ mol^{-1}	R		[21, 35]
				Temperature / °C	
Thermal Expansion Coefficient	8.90e-6	$°C^{-1}$	α	20	[21, 35]
	1.10e-5			1500	
	1.10e-5			1620	
	0.0			1653	
	0.0			2000	

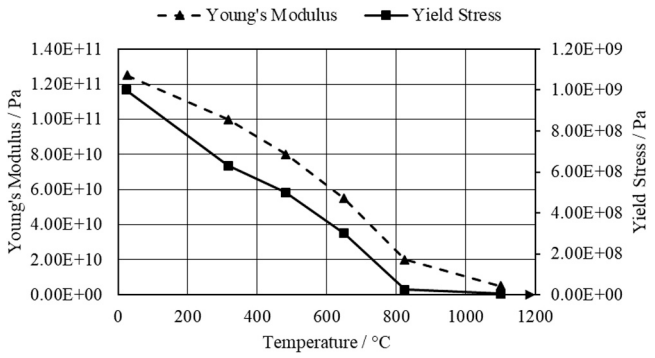

Fig. 4. Yield stress and Young's modulus as a function of temperature. Data from [21,35].

Similarly, the works by Ahmad et al. [39], Ganeriwala et al. [21] and Vrancken et al. [40] measured the residual stresses in a part produced by LPBF and obtained a peak residual stress of approximately 700 MPA.

5.2. Experimental measurement of the displacement field after LPBF

To ensure that the initial stress field is representative of the stress field in the real sample, the deformation of the cantilever, presented in Fig. 6 is compared to the same for a real printed cantilever sample. Fig. 7 shows the 3D scan of the cantilever, after it is removed from the build plate by EDM, and the simulated cantilever in the same orientation. This qualitatively shows that the deformation is similar, and as predicted, the bending mostly occurs inside of the z-x-plane. As mentioned earlier, in order to avoid including the effect of the roughness of the surface of the part, a circle is fitted in four positions through the top surface of the 3D scan. This circle is used to represent the displacement of the cantilever. Fig. 8 shows the deflection in the vertical direction along the cantilever, both for the simulations and the circles fitted to the top of the scanned part. The deflection in the simulations deviate in two positions from the measured value. Near the transition from the left-most support and the cantilever beam itself, the simulations slightly under predict the deflection. This is caused by the left-most support, since it will not deform as much as predicted by a fitted circle. Additionally, the FH method, by virtue of its meta-layer approximation, exposes the part to less heating and cooling cycles than the real part. This will also affect the residual stress level in the part. Near the cantilever tip, the deflection in the simulated beam is lower than in its experimental counterpart. This is an indication that the residual stresses resulting from the FH method are smaller, or differently distributed, than from the real LPBF process. This has been confirmed in the work by Bayat et al. [35], who indicate that the post-LPBF stress field can be improved by refining the FH method, for example by converting it to a sequential flash heating. However, the displacement in the model is less than 10% lower than the lower bound on the experimentally obtained deflection. Therefore, the simulated residual stress field is used as input for simulating the stress relaxation heat treatment.

5.3. Evolution of the stress during the stress relaxation simulation

In order to evaluate the evolution of the stresses during the stress relaxation heat treatment, this paragraph will focus on the heat treatment at 670 °C with a dwell time of five hours. Fig. 9 shows the contours of σ11 in the centre of the cantilever at four different points in time during the heat treatment: the initial stress field, after heating up to the desired temperature, after 4.1 h and at the end of the heat treatment. Note that the cantilever was still attached to the baseplate during this heat treatment. As a result, the cantilever is restricted in its movement. However, the presence of the build plate will not affect the stress distribution in the supported beam itself. The effect of the build plate will be most pronounced in the left-most support. The deflection of the tip of the cantilever, on the other hand, is determined by the stress profile in the beam rather than the supports, and therefore the remainder of this section does not focus on the stress in the left-most support or the build plate itself. Indirect validation of this stress field through measuring the displacement after release from the base plate is the subject of the next paragraph.

The reduction in stress at the beginning of the heat treatment has two origins: plastic deformation and creep. Investigating the former, the yield stress decreases as the temperature increases, which can cause yielding in the part. Zhang et al. [41] found that plastic yielding can contribute approximately fifteen percent to the total stress relaxation for welding, indicating that, in order to find an accurate residual stress field, this phenomenon needs to be included. The importance of the role plastic yielding plays in the simulated heat treatment in this work will be

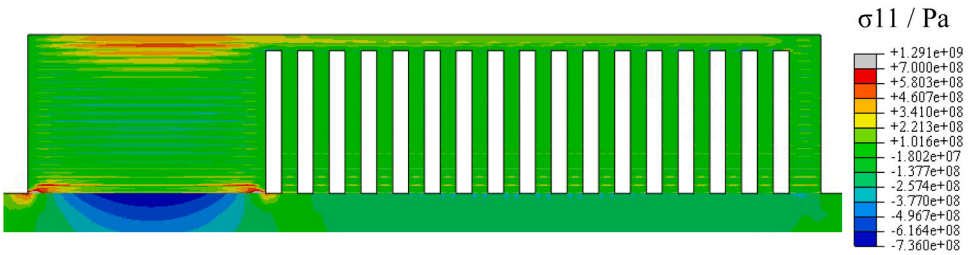

Fig. 5. Normal stress along the cantilever beam at the centre line of the cantilever. This stress field is the result of the primary LPBF simulation using the FH method.

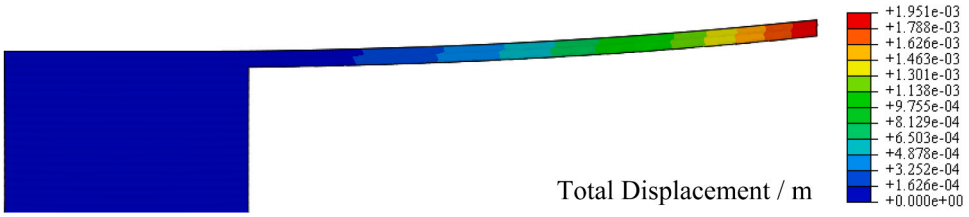

Fig. 6. Displacement of the cantilever after being cut from the build plate.

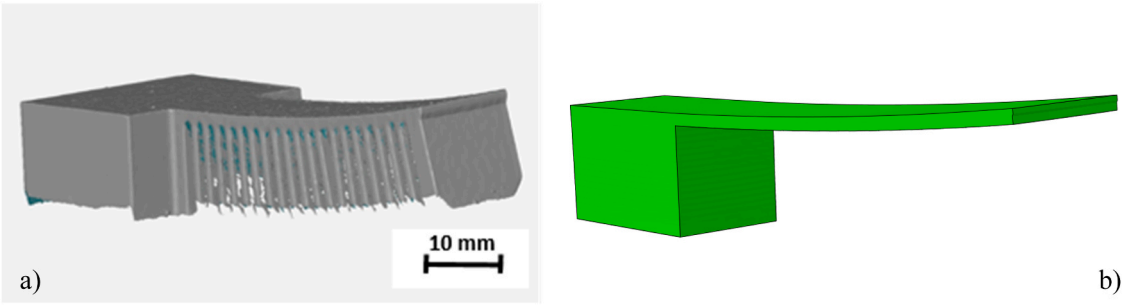

Fig. 7. Displacement of the cantilever. (a) 3D scan of the printed sample from the GOM inspect software, (b) simulated cantilever. The support in the simulated cantilever is removed during the cutting step, but was including during the heat treatment, which is shows in later figures.

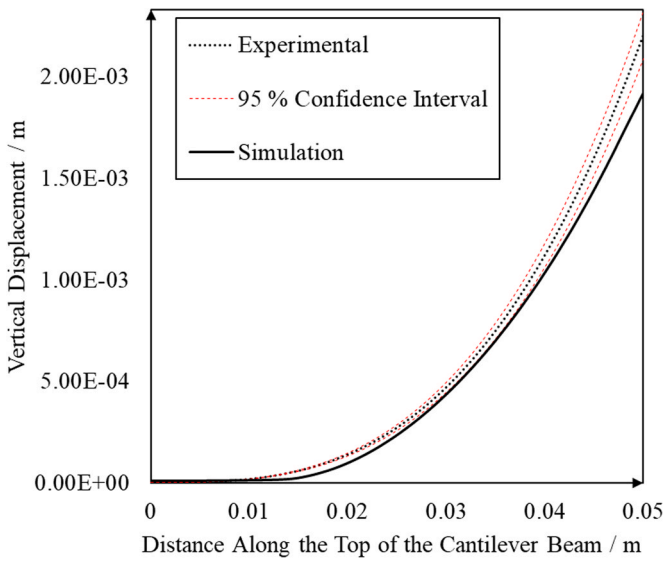

Fig. 8. Vertical deformation along the top of the cantilever, both experimentally (with 95% confidence interval) and from the simulation.

further investigated when analysing the effect of the heat treatment temperature.

Fig. 9 also illustrates the effect of the used creep equation. Not only are the values of the stress in the cantilever lower than just after the LPBF process, but more strikingly, the stress in the leftmost support has been homogenised substantially. Due to the decrease in temperature, and the restriction imposed on the part by the build plate, some new stresses can build up after the heat treatment. Comparing the initial stress contour with the final one shows that the stress is both homogenised and decreased in magnitude.

In order to evaluate the effect of the stress relaxation on the deformation of the cantilever, Fig. 10 shows the total deformation after the chosen heat treatment and after the part is removed from the base plate. The cantilever still bends upwards, but significantly less than before the heat treatment, which is in accordance with the reduction of the residual stress associated with relaxed stresses. After the five-hour heat treatment, the deformation is reduced by approximately 95%.

5.4. Validation of the post-heat treatment deformation

The simulations are able to capture the evolution of the stress according to the proposed creep equation. However, in order to assess the capability of the model to simulate the proposed heat treatment, comparison with experimental results is necessary. Similarly to the validation for the initial stress field, this paper focusses on the deflection as a metric for the macroscopic residual stresses. The displacement of the cantilever following the simulation of the heat treatment at 670 °C at five hours was outlined in the previous section. The experimental measurements were performed on all four printed and post-processed cantilevers, outlined in Section 3. These cantilevers were scanned,

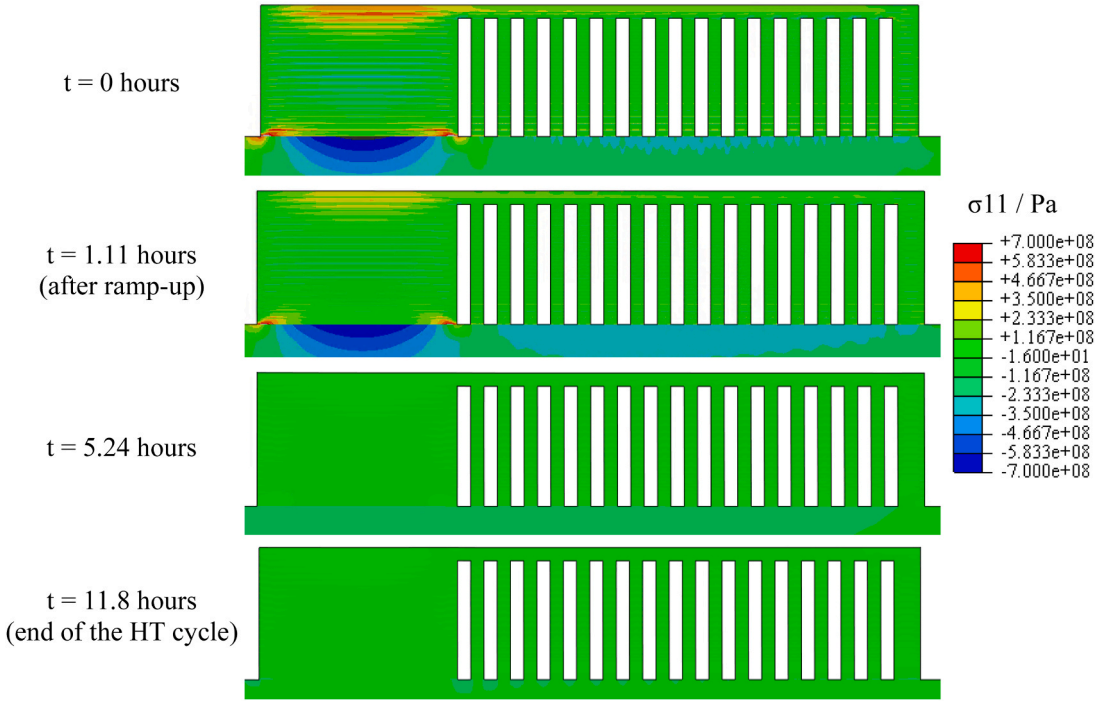

Fig. 9. σ11 at different stages during the heat treatment on the central cross-section during the heat treatment at 670 °C with a dwell time of 300 min.

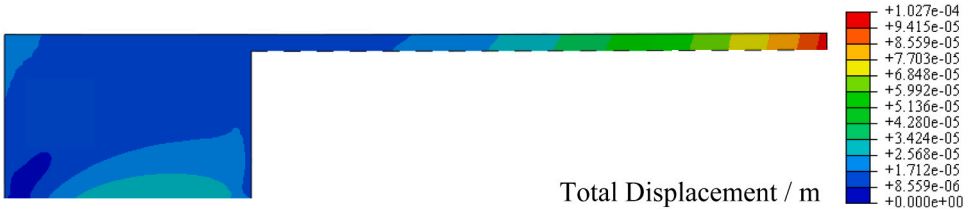

Fig. 10. Displacement after a heat treatment at 670 °C with a dwell time of 5 h, and removal from the base plate.

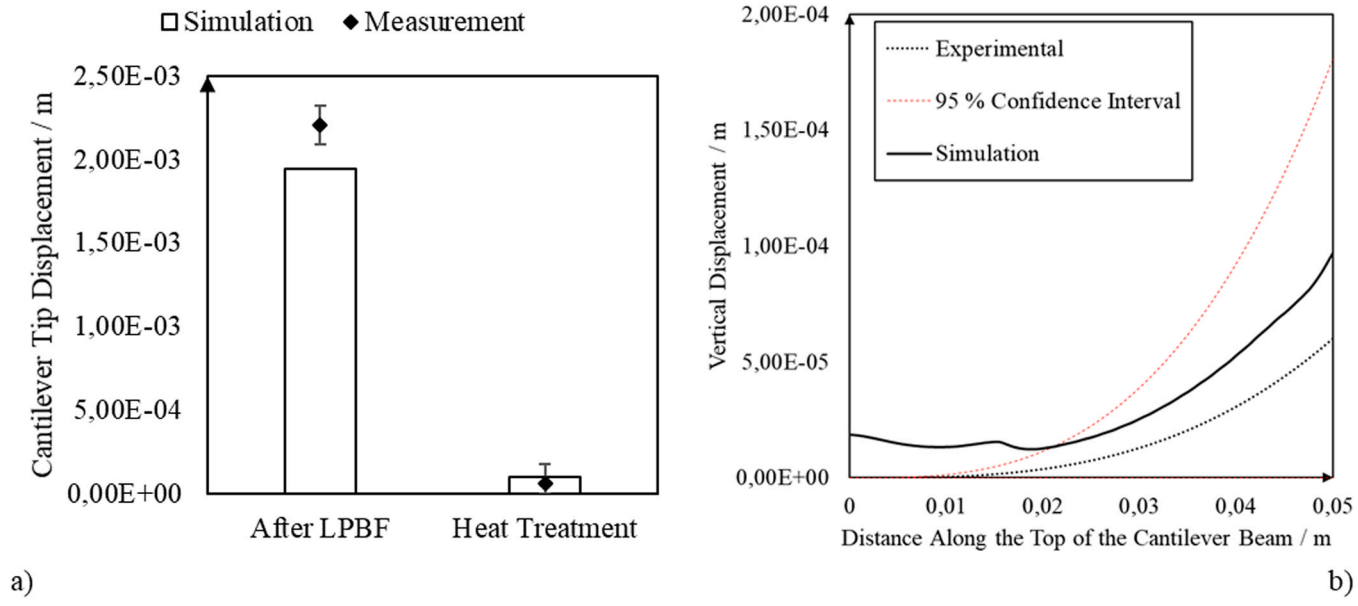

Fig. 11. Validation of the simulations using the measurements on the cantilevers. (a) Displacement of the cantilever tip, both before and after the heat treatment. Both the measured and simulated values are displayed. (b) Displacement at the top surface of the simulated cantilever and aggregated data from the four experimentally printed cantilevers.

after which the displacement of the cantilever tip was extracted in four positions.

Fig. 11 (a) summarises the results from the simulations and the measurements. Both the deflection of the cantilever tip before the heat treatment and after are displayed, and for the experiments, the 95% confidence interval is added. Since the result from a stress relaxation heat treatment in Ti-6Al-4V for the supported cantilever cannot lead to a negative deformation, the lower boundary of the interval is cut off at a deflection of zero. Moreover, the vertical support in the real part will block a downwards deflection by hitting the build plate. As mentioned previously, the deformation of the cantilever after the primary process is slightly lower than the measured value. However, for the displacement of the cantilever tip after the heat treatment, the simulated value of the displacement is similar to the one following from the 3D scans, and serves as validation of the used model. It also indicates that the calculated value of the residual stress resulting from both the real and simulated heat treatment is the same. Moreover, this is the same conclusion obtained by Yan et al. [25], who measured the actual value of the residual stresses using X-ray diffraction measurements. Fig. 11 (b) shows the displacement at the top surface of the simulated cantilever, and the average value of the data extracted from the experimental measurements, together with the 95% confidence. For the first 20 mm, the deflection at the top of the simulated cantilever deviates from the experimental data, but this is the region of the thick left-most support. In the beam itself, the deflection of the top surface lies inside of the confidence interval following from the measurements, indicating that the simulated heat treatment represents the experimental one relatively closely.

5.5. Effect of the parameters on the deformation after cutting from the base plate

The two parameters investigated in the present study are the dwell time and the heat treatment temperature. In Fig. 12, the maximum deformation of the cantilever tip is plotted as a function of dwell time for the different heat treatment temperatures. The general conclusions from this figure are that the deformation decreases for a longer heat treatment and that the decrease is faster when heating at a higher temperature.

The simulation at 510 °C can be used to analyse the influence of plastic yielding on the stress relaxation. Since the heating rate is fixed, the amount of creep during the ramp-up period is limited. Additionally, the shortest heat treatment (nine minutes) also contributes to a small amount of time-dependent strain. This shows that the contribution of the reduction in yield stress during a stress relaxation is approximately one quarter, which is in line with the observation by Zhang et al. [41] in their investigation of stress relaxation on welded pipes.

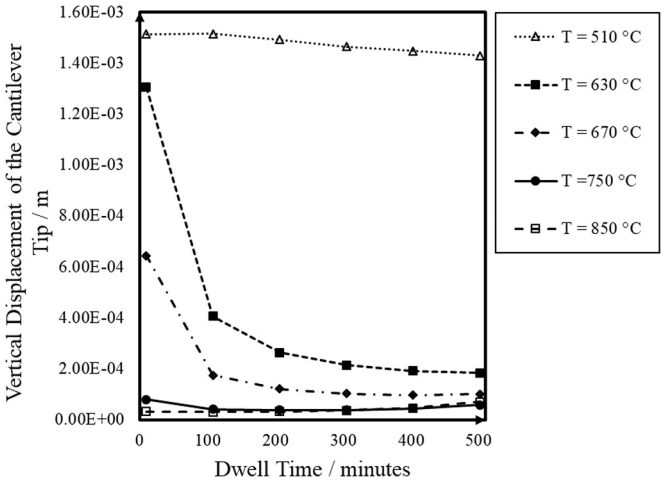

Fig. 12. Displacement of the cantilever as a function of the dwell time, for multiple heat treatment temperatures.

In order to facilitate the discussion on the effect of time and temperature on the final deformations and associated residual stresses, the results for a heat treatment at 670 °C are shown in Fig. 13 and for the heat treatments with a dwell time of 9 min in Fig. 14.

Fig. 13 indicates that there exists an optimal heat treatment time and temperature combination, given certain industrial boundary conditions, which are not investigated in this study and will vary in practice. The curve for the heat treatment at 670 °C, for example, initially decreases fast, and subsequently slows down. This indicates that there is a point of diminishing returns for the heat treatment, after which it becomes too time or energy intensive to reduce the residual stresses even more. The line showing the effect of dwell time on the displacement shows a logarithmic decay. This is a consequence of the creep equation, which was used. High stresses are associated with a large degree of stress relaxation, and as the stresses are relaxed, the driving force for further stress relaxation disappears. This also indicates the location of an ideal heat treatment. Moreover, after 400 min, the deflection of the cantilever increases slightly, which is caused by the redistribution of the stresses. Part of this redistribution could be attributed to numerical errors inherent to the FE method, but the evidence of redistribution of the residual stresses is provided in the next paragraph.

Investigating the effect of the heat treatment temperature in Fig. 14 shows a clear decrease of the deformation as the temperature increases. For the shortest heat treatment, this indicates that the stress relaxation during the ramp-up stage of the heat treatment plays a significant role in determining the final deflections. A similar conclusion was reached by Dong and Hong for stress relaxation after welding [27]. However, during the long heat treatments at high temperatures (above 750 °C), the deflection no longer decreases, but rather increases. To investigate this, Fig. 15 shows the contour of σ11 at the end of a heat treatment at 850 °C with a dwell time of 500 min. Comparing these stress contours with Fig. 5 shows that a significant amount of stress redistribution has taken place. Moreover, the stresses in the beam no longer evolve from tensile at the top to compressive near the bottom, and therefore, this stress state of the cantilever will no longer dictate its deformation. The deflection of the tip is now caused by the deformation in the left-most support, which is driven by the region of higher tensile stress at its top surface.

Fig. 12 and 15 also show that it is difficult to remove all residual stresses with the chosen stress relaxation model. The stress relaxation is modelled using a power-law creep equation, which will never reduce the stresses to zero. Additionally, the chosen equation, used to represent the stress relaxation, does lump together certain aspects of the real heat treatment into a two-parameter model. This also limits the range of applicability for the model. For example, below approximately 350 °C, the original microstructure will not decompose [42], and above the β transus temperature, the phase transformation behaviour might start to deviate from the assumed one [13]. These mechanisms are not captured

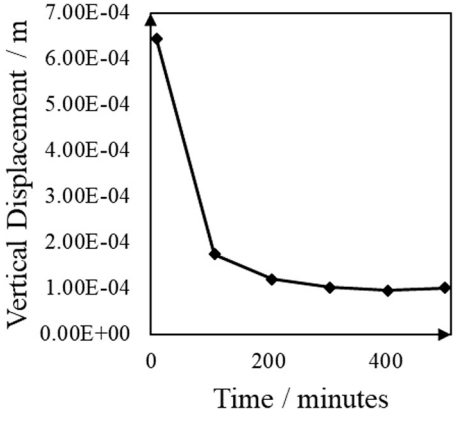

Fig. 13. Displacement as a function of time for a heat treatment at 670 °C.

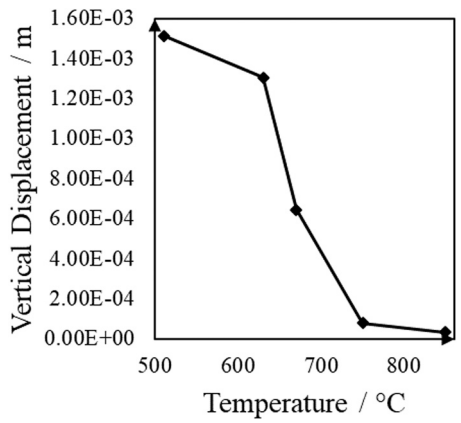

Fig. 14. Displacement as a function of temperature for a heat treatment with a dwell time of 9 min. Note that the horizontal axis starts at 500 °C.

by the current model, and would require additional experiments to find its input parameters. As indicated previously, redistribution of the stress during the highest temperature heat treatments can also increase the displacement of the cantilever tip, and can be confused with incomplete relaxation of the residual stress.

Comparing the results in this paragraph with results from experimental stress relaxation studies allows to validate the use of a Norton's power law based creep equation for modelling the change in residual stress. Wang et al. [16] used neutron diffraction to find a reduction of approximately 90% for a heat treatment at 600 °C after 100 min. Similar to the conclusion from the results presented in Fig. 14, they show that heat treating at a higher temperature (700 °C) leads to a more rapid reduction in the residual stress. Similarly, Ter Haar and Becker [43] show for a range of temperatures from 427 °C to 610 °C and dwell times from 5 min to 30 h that the residual stresses initially decrease rapidly, while even at 610 °C for 30 h some residual stresses remain in the part. Heating at higher temperatures, similarly as in this study, show that a higher heat treatment temperature results in a more rapid relaxation of the stress. Finally, Rae and Rahimi [44] measured the evolution of the residual stresses during a stress relaxation heat treatment, and show a decay in residual stress similar to the simulated outcome shown in Fig. 12, but also highlight a large variation in the results from different data sources for stress relaxation.

5.6. Determination of the process map

The results presented in the previous sections allow for an investigation into the process window. Moreover, generating a contour plot of the deformation as a function of temperature and dwell time will result in a process plot, which indicates a window of process condition under which minimal deflection after the heat treatment can be expected. Fig. 16 shows a process map derived from the performed simulations. The displacement is used as an estimating value for the reduction in the residual stresses.

This process map allows for a rapid determination of the heat treatment window for the given geometry, and can be used to determine the optimal heat treatment to get a specific reduction of the residual stresses. This reduces the need for both expensive trial-and-error studies or comprehensive high-fidelity models. However, this process map only directly applies to a situation where the residual stresses are at the level indicated in Fig. 5. Currently, there is no data available investigating the sensitivity of a LPBF post-process model on the initial residual stresses, and this can be a topic for future investigations.

6. Conclusion

In the present work, a creep model is used to simulate a stress relaxation heat treatment, which is often used to reduce the deformations after the LPBF process. After the initial stress field is obtained from a simulation using the FH method, and after validation of this stress field, this model is implemented in commercial finite elements software. In order to evaluate the influence of the different heat treatment parameters, a number of heat treatments are simulated using this model, and the results are the following:

- The stress relaxation can be sufficiently accurately approximated using the chosen temperature dependent creep equation. This conclusion is enforced by the validation via experimental results.
- Plastic yielding contributes to a minimal amount of approximately 25% of the reduction in the residual stresses.
- Heat treating at low temperatures only results in a small reduction of the residual stresses, and therefore post-processing the part at higher temperatures is more efficient. However, due to the exponential nature of the creep equation, there is a point of diminishing return, where higher heat treatment temperatures and longer heat treatment times not necessarily lead to a significant reduction in the residual stress. This is caused in part by using creep to represent stress relaxation during a heat treatment.

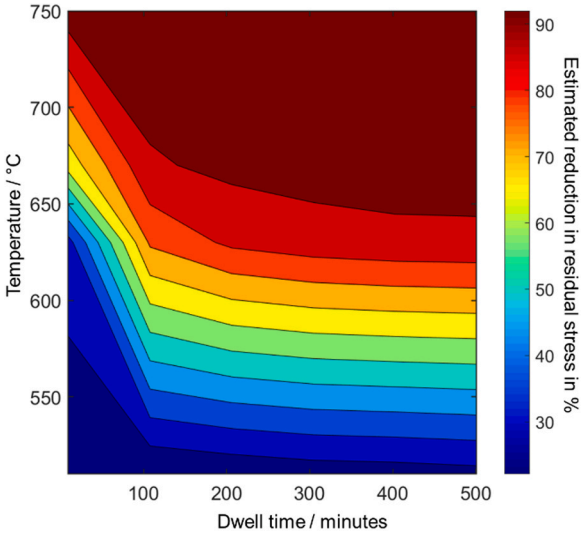

Fig. 16. Process map for post-LPBF heat treatments.

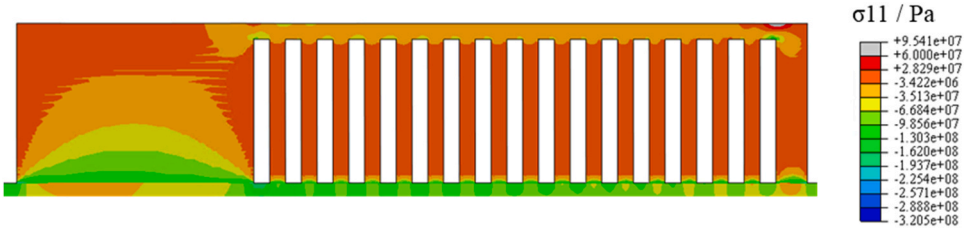

Fig. 15. σ11 the end of a heat treatment at 850 °C with a dwell time of 9 min.

- A process map is constructed to summarise the results from the simulations. This process map shows how simulations, like the ones performed in this paper, can be applied directly to find the optimal heat treatment conditions. However, additional investigations into the effect of the magnitude of the initial residual stress are required.

CRediT authorship contribution statement

David De Baere: Conceptualization, Methodology, Validation, Formal analysis, Investigation, Writing - original draft, Writing - review & editing, Visualization. **Pierre Van Cauwenbergh**: Methodology, Validation, Investigation, Writing - Review & Editing. **Mohamad Bayat**: Conceptualization, Methodology, Writing - Review & Editing. **Sankhya Mohanty:** Writing - Review & Editing, Supervision. **Jesper Thorborg**: Conceptualization, Writing - Review & Editing, Supervision, Funding acquisition. **Lore Thijs**: Writing - Review & Editing, Supervision, Funding acquisition. **Brecht Van Hooreweder:** Writing - Review & Editing, Supervision. **Kim Vanmeensel:** Writing - Review & Editing, Supervision. **Jesper Hattel:** Conceptualization, Writing - Review & Editing, Supervision, Funding acquisition.

Declaration of Competing Interest

The authors declare that they have no known competing financial interests or personal relationships that could have appeared to influence the work reported in this paper.

Acknowledgements

This project has received funding from the European Union's Horizon 2020 research and innovation programme under the Marie Skłodowska-Curie grant agreement No 721383. P. Van Cauwenbergh acknowledges 3D Systems Leuven and Flanders Innovation & Entrepreneurship for funding the Baekeland Research Project HBC.2016.0614 "Tailoring heat treatments for laser powder bed fusion processed metals".

References

[1] M. Markl, C. Körner, Multiscale modeling of powder bed–based additive manufacturing, Annu. Rev. Mater. Res. 46 (2016) 93–123, https://doi.org/10.1146/annurev-matsci-070115-032158.
[2] J.L. Bartlett, X. Li, An overview of residual stresses in metal powder bed fusion, Addit. Manuf. 27 (2019) 131–149, https://doi.org/10.1016/j.addma.2019.02.020.
[3] C. Li, J.F. Liu, X.Y. Fang, Y.B. Guo, Efficient predictive model of part distortion and residual stress in selective laser melting, Addit. Manuf. 17 (2017) 157–168, https://doi.org/10.1016/j.addma.2017.08.014.
[4] P. Mercelis, J. Kruth, Residual stresses in selective laser sintering and selective laser melting, Rapid Prototyp. J. 12 (2006) 254–265, https://doi.org/10.1108/13552540610707013.
[5] B. Vrancken, S. Buls J.P. Kruth Van, J. Humbeeck, Influence of preheating and oxygen content on selective laser melting of Ti6Al4V, Proceedings of the 16th RAPDASA Conference; 2015.
[6] L. Parry, I.A. Ashcroft, R.D. Wildman, Understanding the effect of laser scan strategy on residual stress in selective laser melting through thermo-mechanical simulation, Addit. Manuf. 12 (2016) 1–15, https://doi.org/10.1016/j.addma.2016.05.014.
[7] M. Shiomi, K. Osakada, K. Nakamura, T. Yamashita, F. Abe, Residual stress within metallic model made by selective laser melting process, CIRP Ann. Manuf. Technol. 53 (2004) 195–198, https://doi.org/10.1016/S0007-8506(07)60677-5.
[8] D.N. Croft, Types of heat treatment. Heat Treat. Welded Steel Structure, Woodhead Publishing, 1996, pp. 9–20, https://doi.org/10.1016/B978-1-85573-016-8.50007-8.
[9] A.K. Syed, B. Ahmad, H. Guo, T. Machry, D. Eatock, J. Meyer, et al., An experimental study of residual stress and direction-dependence of fatigue crack growth behaviour in as-built and stress-relieved selective-laser-melted Ti6Al4V, Mater. Sci. Eng. A 755 (2019) 246–257, https://doi.org/10.1016/j.msea.2019.04.023.
[10] T. Vilaro, C. Colin, J.D. Bartout, As-fabricated and heat-treated microstructures of the Ti-6Al-4V alloy processed by selective laser melting, Met. Mater. Trans. A Phys. Met. Mater. Sci. 42 (2011) 3190–3199, https://doi.org/10.1007/s11661-011-0731-y.
[11] G. Sin, K.V. Gernaey, Data handling and parameter estimation, Exp. Methods Wastewater Treat. 9781780404 (2016) 201–234.
[12] M. Yakout, M.A. Elbestawi, S.C. Veldhuis, S. Nangle-Smith, Influence of thermal properties on residual stresses in SLM of aerospace alloys, Rapid Prototyp. J. 26 (2020) 213–222, https://doi.org/10.1108/RPJ-03-2019-0065.
[13] D. De Baere, S. Mohanty, J.H. Hattel, Microstructural modelling of above β-transus heat treatment of additively manufactured Ti-6Al-4V using cellular automata, Mater. Today Commun. 24 (2020), 101031, https://doi.org/10.1016/j.mtcomm.2020.101031.
[14] S. Liu, Y.C. Shin, Additive manufacturing of Ti6Al4V alloy: a review, Mater. Des. 164 (2019), 107552, https://doi.org/10.1016/j.matdes.2018.107552.
[15] J.-P. Kruth, J. Deckers, E. Yasa, R. Wauthlé, Assessing and comparing influencing factors of residual stresses in selective laser melting using a novel analysis method, Proc. Inst. Mech. Eng. Part B J. Eng. Manuf. 226 (2012) 980–991, https://doi.org/10.1177/0954405412437085.
[16] Z. Wang, A.D. Stoica, D. Ma, A.M. Beese, Stress relaxation behavior and mechanisms in Ti-6Al-4V determined via in situ neutron diffraction: application to additive manufacturing, Mater. Sci. Eng. A 707 (2017) 585–592, https://doi.org/10.1016/j.msea.2017.09.071.
[17] H. Ali, L. Ma, H. Ghadbeigi, K. Mumtaz, In-situ residual stress reduction, martensitic decomposition and mechanical properties enhancement through high temperature powder bed pre-heating of selective laser melted Ti6Al4V, Mater. Sci. Eng. A 695 (2017) 211–220, https://doi.org/10.1016/j.msea.2017.04.033.
[18] D.J. Corbin, A.R. Nassar, E.W. Reutzel, A.M. Beese, P. Michaleris, Effect of substrate thickness and preheating on the distortion of laser deposited ti-6al-4v, J. Manuf. Sci. Eng. Trans. ASME 140 (2018) 1–9, https://doi.org/10.1115/1.4038890.
[19] G. Vastola, G. Zhang, Q.X. Pei, Y.W. Zhang, Controlling of residual stress in additive manufacturing of Ti6Al4V by finite element modeling, Addit. Manuf. 12 (2016) 231–239, https://doi.org/10.1016/j.addma.2016.05.010.
[20] E.R. Denlinger, P. Michaleris, Effect of stress relaxation on distortion in additive manufacturing process modeling, Addit. Manuf. 12 (2016) 51–59, https://doi.org/10.1016/j.addma.2016.06.011.
[21] R.K. Ganeriwala, M. Strantza, W.E. King, B. Clausen, T.Q. Phan, L.E. Levine, et al., Evaluation of a thermomechanical model for prediction of residual stress during laser powder bed fusion of Ti-6Al-4V, Addit. Manuf. 27 (2019) 489–502, https://doi.org/10.1016/j.addma.2019.03.034.
[22] D. De Baere, M. Bayat, S. Mohanty, J.H. Hattel, Part-scale mechanical modelling of LPBF including microstructural evolution effects part-scale mechanical modelling of LPBF including microstructural evolution effects, IOP Conf. Ser. Mater. Sci. Eng. 861 (2020), 012013, https://doi.org/10.1088/1757-899X/861/1/012013.
[23] D. De Baere, M. Moshiri, S. Mohanty, G. Tosello, J.H. Hattel, Numerical investigation into the effect of different parameters on the geometrical precision in the laser-based powder bed fusion process chain, Appl. Sci. 10 (2020), https://doi.org/10.3390/app10103414.
[24] R.J. Williams, F. Vecchiato, J. Kelleher, M. Wenman, Effects of heat treatment and build orientation on residual stresses in the laser powder bed fusion of 316L stainless steel: finite element predictions and neutron diffraction measurements, J. Mater. Process Technol. (2020).
[25] G. Yan, A. Crivoi, Y. Sun, N. Maharjan, X. Song, F. Li, et al., An Arrhenius equation-based model to predict the residual stress relief of post weld heat treatment of Ti-6Al-4V plate, J. Manuf. Process 32 (2018) 763–772, https://doi.org/10.1016/j.jmapro.2018.04.004.
[26] P. Dong, S. Song, J. Zhang, Analysis of residual stress relief mechanisms in post-weld heat treatment, Int J. Press Vessel Pip. 122 (2014) 6–14, https://doi.org/10.1016/j.ijpvp.2014.06.002.
[27] P. Dong, J.K. Hong, Residual Stress Relief Post Weld Heat Treat. (2009) 321–329, https://doi.org/10.1115/pvp2008-61210.
[28] H. Alberg, D. Berglund, Comparison of plastic, viscoplastic, and creep models when modelling welding and stress relief heat treatment, Comput. Methods Appl. Mech. Eng. 192 (2003) 5189–5208, https://doi.org/10.1016/j.cma.2003.07.010.
[29] W. Rae, Thermo-metallo-mechanical modelling of heat treatment induced residual stress in Ti–6Al–4V alloy, Mater. Sci. Technol. 35 (2019) 747–766, https://doi.org/10.1080/02670836.2019.1591031.
[30] J.P. Kruth, L. Froyen, J. Van Vaerenbergh, P. Mercelis, M. Rombouts, B. Lauwers, Selective laser melting of iron-based powder, J. Mater. Process Technol. 149 (2004) 616–622, https://doi.org/10.1016/j.jmatprotec.2003.11.051.
[31] I. Setien, M. Chiumenti, S. van der Veen, M. San Sebastian, F. Garciandía, A. Echeverría, Empirical methodology to determine inherent strains in additive manufacturing, Comput. Math. Appl. 78 (2019) 2282–2295, https://doi.org/10.1016/j.camwa.2018.05.015.
[32] M.E. Kassner, Fundamentals of Creep in Metals and Alloys, third ed., Butterworth Heinemann, Oxford, 2015.
[33] F.H. Norton, The Creep of Steel at High Temperatures, third ed., McGraw-Hill Book Company, Inc, New York, 1929.
[34] A. Coro, L.M. Macareno, J. Aguirrebeitia, De, L.N.L. Lacalle, A methodology to evaluate the reliability impact of the replacement of welded components by additive manufacturing spare parts, in: Metals, 9, 2019, pp. 1–19, https://doi.org/10.3390/met9090932.
[35] M. Bayat, C.G. Klingaa, S. Mohanty, D. De Baere, J. Thorborg, N. Skat Tiedje, et al., Part-scale thermo-mechanical modelling of distortions in L-PBF - Analysis of the sequential flash heating method with experimental validation, Addit. Manuf. (2020), 101508.
[36] M. Peters, J. Hemptenmacher, J. Kumpfert, C. Leyens, Structure and properties of titanium and titanium alloys, in: C. Leyens, M. Peters (Eds.), Titanium and Titanium Alloys: Fundamentals and Applications, Wiley-VCH Verlag GmbH & Co, Weinheim, 2003, pp. 1–35.

[37] Q. Chen, X. Liang, D. Hayduke, J. Liu, L. Cheng, J. Oskin, et al., An inherent strain based multiscale modeling framework for simulating part-scale residual deformation for direct metal laser sintering, Addit. Manuf. 28 (2019) 406–418, https://doi.org/10.1016/j.addma.2019.05.021.
[38] I. Yadroitsava, S. Grewar, D. Hattingh, I. Yadroitsev, Residual stress in SLM Ti6Al4V alloy specimens, Mater. Sci. Forum 828–829 (2015) 305–310, https://doi.org/10.4028/www.scientific.net/MSF.828-829.305.
[39] B. Ahmad, S.O. van der Veen, M.E. Fitzpatrick, H. Guo, Residual stress evaluation in selective-laser-melting additively manufactured titanium (Ti-6Al-4V) and inconel 718 using the contour method and numerical simulation, Addit. Manuf. 22 (2018) 571–582, https://doi.org/10.1016/j.addma.2018.06.002.
[40] B. Vrancken, V. Cain, R. Knutsen, J. Van Humbeeck, Residual stress via the contour method in compact tension specimens produced via selective laser melting, Scr. Mater. 87 (2014) 29–32, https://doi.org/10.1016/j.scriptamat.2014.05.016.
[41] J. Zhang, P. Dong, S. Song, Stress relaxation behavior in PWHT of welded components, Am. Soc. Mech. Eng. Press. Vessel. Pip. Div. Conf. (2011) 673–679, https://doi.org/10.1115/pvp2011-57826.
[42] F.X. Gil Mur, D. Rodríguez, J. a Planell, Influence of tempering temperature and time on the α′-Ti-6Al-4V martensite, J. Alloy. Compd. 234 (1996) 287–289, https://doi.org/10.1016/0925-8388(95)02057-8.
[43] G.M. Ter Haar, T.H. Becker, Low temperature stress relief and martensitic decomposition in selective laser melting produced Ti6Al4V, Mater. Des. Process Commun. (2020) 2–7, https://doi.org/10.1002/mdp2.138.
[44] W. Rae, S. Rahimi, Effect of stress relaxation on the evolution of residual stress during heat treatment of Ti-6Al-4V, The 14th World Conference on Titanium 11001 2020 9 12.